actuators

MDPI

Article

The Design and Performance Investigation of a Split Four-Track Water-Jet Cleaning Robot for Steel Gate Panels

Zhenhua Duan [1], Guisheng Fang [1,*], Gaoping Shi [1], Heng Qian [1], Jiayi Cui [2] and Junhao Zhang [3]

[1] School of Mechanical Engineering, Zhejiang University of Water Resources and Electric Power, Hangzhou 310018, China; duanzh@zjweu.edu.cn (Z.D.); shigp@zjweu.edu.cn (G.S.); qianh@zjweu.edu.cn (H.Q.)
[2] College of Metrology Measurement and Instrument, China Jiliang University, Hangzhou 310018, China; p22020854013@cjlu.edu.cn
[3] School of Mechanical Engineering, Zhejiang Sci-Tech University, Hangzhou 310018, China; 2023220504068@mails.zstu.edu.cn
* Correspondence: fanggsh@zjweu.edu.cn

Abstract: Steel gates are widely used in river and sea engineering to ensure water retention and flow regulation. Due to the attachment and the alternation of dry and wet environments, water retention easily causes corrosion and destruction, while the attachment is mainly cleaned manually at present. Based on stable adsorption, wall adaptability, and movement ability, a split four-track cleaning robot was developed. The split structure combined with a body swing and torsion mechanism can increase the degree of freedom of attitude adjustment and realize stable crawling of the curved panel. Considering the impact force of the water jet during cleaning, mechanical analysis of robot instability and driving torque on a curved surface was constructed to solve the problem of safe adsorption and flexible movement. A remote control system is constructed to complete the cleaning operation, and the coordination relationship between cleaning and crawling speed is analyzed. The performance test results show that the robot can crawl flexibly and stably on a curved surface, and the crawling speed can be greater than 0.052 m/s when the load is less than 5 kg. A continuous cleaning process has an obvious effect on silt and shellfish attachments, and the robot can meet the actual operational needs. The design process can help in the development of this kind of robot.

Keywords: water-jet cleaning robot; split structure; adaptive regulation; steel gate panels; shellfish

check for updates

Citation: Duan, Z.; Fang, G.; Shi, G.; Qian, H.; Cui, J.; Zhang, J. The Design and Performance Investigation of a Split Four-Track Water-Jet Cleaning Robot for Steel Gate Panels. *Actuators* **2024**, *13*, 528. https://doi.org/10.3390/act13120528

Academic Editor: Ioan Doroftei

Received: 18 November 2024
Revised: 13 December 2024
Accepted: 19 December 2024
Published: 20 December 2024

Copyright: © 2024 by the authors. Licensee MDPI, Basel, Switzerland. This article is an open access article distributed under the terms and conditions of the Creative Commons Attribution (CC BY) license (https://creativecommons.org/licenses/by/4.0/).

1. Introduction

Hydraulic steel gates, as steel structural components employed for regulating water level and water flow in river and sea engineering projects, such as water resource allocation [1], port and ship lock management [2,3], flood control, and tide blocking [4], constitute a vital component of hydraulic structures like hydropower stations, ship locks, and pumping stations [5]. They constitute approximately 20% of the total cost of the entire hydraulic engineering, and in certain hydraulic engineering projects, they might even account for more than half. The gate panel serves as the primary water-blocking component. During operation, the surface of the panel situated underwater is influenced by water quality, aquatic algae, and other biological organisms, thereby accumulating silt, moss, shellfish, and the like to varying extents. Once the panel leaves the water's surface, the accumulated substances and the alternating dry and wet environments can give rise to rust and even damage on the panel surface, which adversely affects the structural integrity, strength, and bearing capacity of the gate [6]. Hence, in routine maintenance, the gate panel, especially the water-blocking surface, needs to be regularly cleaned to remove surface attachments. Additionally, for routine safety inspections of the panel, it is requisite to clear the surface accumulations in advance to enhance the accuracy of the safety inspections.

Traditional steel gate panel cleaning was predominantly carried out manually using tools like scrapers and brooms, which was inefficient and susceptible to causing damage to the panel surface. Water-jet cleaning is a physical cleaning approach that employs high-pressure water streams to strike and scour the surface of structures for the removal of attachments and grime. Initially, it was predominantly utilized for cleaning contaminated surfaces with handheld spray guns or spray rods, yet it was labor-intensive and entailed high labor costs. In recent years, concomitant with the evolution of robot technology, a number of water-jet cleaning apparatuses have been developed, and climbing robots furnished with cleaning equipment have been extensively employed in cleaning operations on ships, oil tanks, pipelines, etc.

Huang et al. [7] designed and manufactured a self-rotating cleaning device, analyzed the submerged cavitation effect of different nozzles via numerical simulation, and evaluated the cleaning efficacy and parameters of the cleaning device. Wei et al. [8] put forward a design for an underwater ship-hull-cleaning robot that integrates conventional mechanical cleaning and high-pressure jet cleaning approaches. The robot is capable of mechanically cleaning the majority of the ship hull initially and subsequently employs cavitation jet cleaning to deeply remove residues, thereby attaining efficient and damage-free comprehensive cleaning. A fluid simulation experiment was carried out using Fluent to ensure the robot meets the cleaning requirements of offshore platforms. Orozco-Magdaleno et al. [9] devised a three-wheel mobile cleaning robot that utilizes a water-jet gun installed on a gimbal to fulfill cleaning tasks. Based on statical analysis, the influences of the repulsive force and reaction force of the water jet on the robot were studied. Yan et al. [10] proposed a pipeline wall-cleaning robot that employs scrapping, brushing, and suction for collecting impurities within the pipeline. Through fluid simulation and experiments, the target distance was approximately 25 mm and the injection angle was 15° to attain the optimal cleaning effect. At this juncture, the maximum shearing force exerted on the target surface was approximately 0.11 MPa. Feng et al. [11] devised a pipe-cleaning robot that eliminates sediments in the pipe by equipping it with a high-pressure water jet and a pipe-cleaning system and analyzed and verified the IPCR mechanism of the high-pressure water jet. Yang et al. [12] proposed a wheeled wall-climbing robot using push-shovel cleaning technology to scrape away marine biofouling, which can adapt to surfaces with a curvature above 3 m and has a good effect on removing barnacles. Its weight is greater than others, which is about 50 kg. Liao et al. [13] undertook research on the intelligent cleaning and rust removal of oil storage tanks through cavitation water-jet technology. A mechanical support frame was installed precisely at the center of the bottom of the oil storage tank, and six sets of cavitation-cleaning nozzles were uniformly distributed on the support frame. The inner wall of the oil storage tank was cleansed by the rotation of the support frame. Yi et al. [14] designed a ship-wall rust-removal and climbing robot with permanent magnet and vacuum-mixed adsorption, which has the characteristics of large load and self-weight. The robot dynamics model was established with the plane as the target, and optimization and simulation analysis were carried out. Zhang et al. [15] designed an oil-tank-wall cleaning robot with a three-wheel wheel configuration, which was capable of conducting full-direction water-jet cleaning operations via the rotation and pitch of a three-degrees-of-freedom mechanical arm. Hu et al. [16] designed a tracked high-pressure water-jet rust-removal climbing robot by analyzing the relationship between structural parameters and magnetic adhesion force and optimizing the adhesion scheme.

From the perspective of the structure and function of the existing climbing cleaning robots, tracked and wheel-type crawling mechanisms are predominantly employed, and they are all of the monolithic structure type. Although they possess certain wall-surface adaptability, their adaptability direction is relatively limited. Concurrently, under the same cleaning operation conditions, in order to guarantee that the robot has sufficient adhesion force, the structure of the wheel-type robot is frequently larger than that of the tracked robot.

Owing to the diverse structure of steel gates, wall-crawling operations impose heightened requirements on the adaptability and versatility of automation equipment. Steel gates commonly employed in river and sea engineering projects are mainly planar and curved (as shown in Figure 1) in accordance with their structural forms. For full-position operation on the curved panel, the cleaning robot is obliged to achieve stable adhesion on the panel along with a certain wall-adaptability adjustment capacity. Simultaneously, adequate load capacity constitutes a guarantee for the robot's safe operation under diverse water-jet cleaning pressures. Hence, novel requirements have been stipulated for the robot's self-adaptive adjustment of the structure posture and the overall load capacity during climbing. During the operation of the gate, the panel attachments fluctuate in accordance with the water body and ecological environment. Through field investigations, the attachments are categorized into silt, secretions of aquatic plants, and shellfish. According to manual operation experience, the water impact force necessary for the removal of shellfish is the greatest.



(**a**) (**b**) (**c**) (**d**)

Figure 1. Steel gates applied in river and sea engineering; (**a**) plane steel gate; (**b**) radial steel gate; (**c**) gate of the ship lock; (**d**) the attachment.

In response to the actual requirements and extant problems, the design and performance study of a water-jet cleaning robot suitable for steel gate panels in river and sea engineering is carried out. Through structural design, theoretical analysis, and performance testing, the cleaning robot can effectively eliminate various deposits and adhesions that have accumulated on the surfaces of the gate panels, thereby mitigating surface damage and prolonging the service life of the gate.

The rest of the work is arranged as follows. Section 2 puts forward the structure's scheme based on the design requirements of the cleaning robot and carries out the adaptability analysis of the panel surface. On this basis, Section 3 carries out the mechanical analysis of the robot. In Section 4, the control system and its composition are designed to realize the remote control of the cleaning operation, and the prototype performance test is carried out in Section 5. Finally, the conclusion of this study is drawn in Section 6.

2. Overall Structure Design and Operating Principle

2.1. Design Requirements

The water-jet cleaning robot is requisite for the cleaning operation at the gate, and its working components are categorized into a panel part and a ground part. The climbing robot is initially placed in a suitable position on the panel. To avert unexpected instability and falling during the operation, the robot is linked to the hydraulic structure at the top of the gate via a safety rope. The ground part is furnished with a high-pressure pump set and connected to the robot's spray gun through a water pipe. A direct-current power supply is also coupled to the robot controller by means of a cable. Additionally, to alleviate the robot's load, the water pipe and cable are hoisted by a lifting rope from the top of the gate, and a flat steel gate panel-cleaning operation is shown in Figure 2.

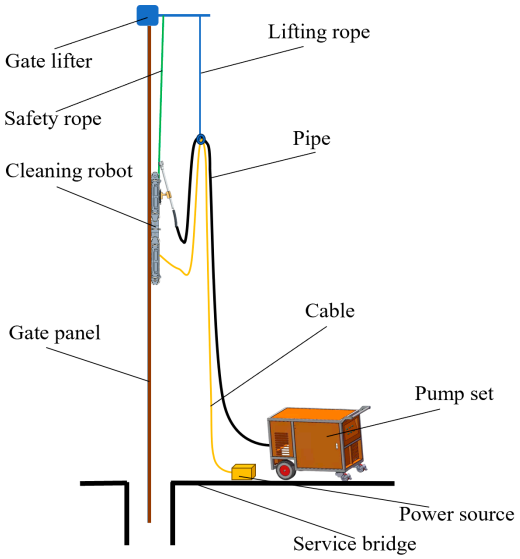


Figure 2. The schematic illustration of the operation scene of the cleaning robot.

Distinct from conventional wall-climbing robots, cleaning robots will encounter a considerable reaction force during the process of panel cleaning. Hence, the robot body is expected to possess a specific load capacity, and the rated load is set at 5 kg. Among the structural forms of steel gates, the predominant ones are plane panels and curved panels. In light of the current advancements in relevant research on radial steel gates [17–21], the overall curvature radius of gates employed in dams and reservoirs is typically larger (ranging from 12 m to 32 m), whereas the curvature radius of gates utilized in small river channels is smaller (varying from 2 m to 5 m). When the adhesion area of the robot remains unaltered, the greater the curvature radius, the narrower the adjustment range of the robot's posture. Consequently, the smaller the curvature radius, the higher the demands for adhesion performance. With the aim of enhancing the versatility of the cleaning robot for diverse wall surfaces, the curvature radius of the curved panel is set at $R \geq 2000$ mm. Taking into account the working efficiency and crawling stability of the robot, the crawling speed is determined to be greater than 0.05 m/s.

2.2. Structure Composition

The main water-blocking component of the steel gate is the panel, and the conventional cleaning operations are mainly aimed at cleaning the dirty surface on the panel. The steel sluice gate panel mainly consists of flat and curved structures; thus, the cleaning robot must be capable of climbing and adhering to both flat and curved surfaces. To endow the robot with the capacity to adaptively adjust its crawling on complex wall surfaces, the robot body was devised with a multi-degree-of-freedom beam frame structure at both the front and rear so that it forms a split structure for passive adaptation to wall surfaces of different curvatures. Concurrently, the flipping structure of the front and rear beam frames could facilitate the 90° wall-transition operation. To guarantee that the robot could remain stably adhered during the cleaning process even when exposed to the reactive force of the jet stream, the crawling mode adopted four sets of tracked adhesion mechanisms. The spray rod was positioned at the front end of the robot, and by adjusting the position of the base, the spray rod could pitch and rotate left and right, attaining multi-angle water-jet cleaning. Based on this design notion, the overall structure of the panel water-jet cleaning robot is presented in Figure 3, mainly consisting of the mobile mechanism, connection frame, spray rod, base, motor controller, base controller, etc.

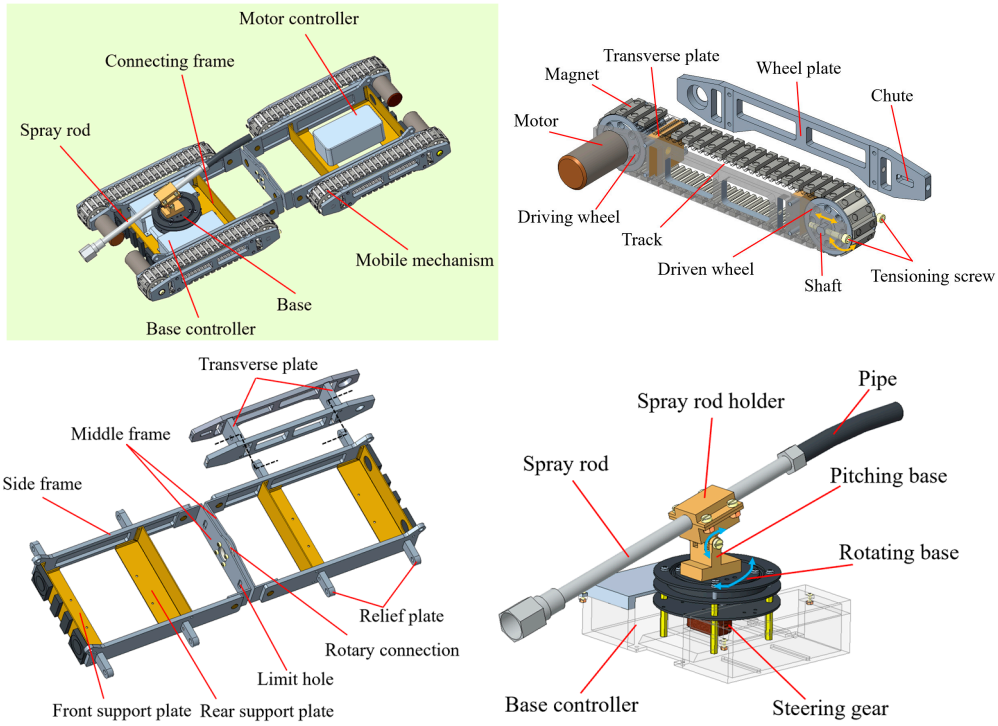


Figure 3. The overall structure of the robot.

The mobile mechanism is accomplished through the track and the permanent magnets positioned on its outer side. The motor directly drives the driving wheel, which is fixed and supported by two wheel plates and interconnected by two transverse plates between them. The chute is established on the wheel plate at the end of the driven wheel, and by rotating the tensioning screws, the driven wheel shaft can move back and forth within the chute, thereby achieving the tensioning of the track. The connection frame serves as the supporting component for each part of the cleaning robot. To enhance the flexibility of the robot's adaptation to complex wall surfaces, the connecting frame adopts a symmetrical split structure with front and rear frames, composed of side frames and middle frames. Front and rear support plates are placed between the side frames to support the cleaning components and the motor controller, etc. There are two protruding plates on the side frames, which are linked to the transverse plates of the mobile mechanism via pins, enabling the mobile mechanism to tilt up and down at a certain angle. The middle frames are divided into two groups and are fastened on the opposite sides of the circular axle plate, and the ends of the middle frames are hinged to the side frames, allowing the connection frame to adjust its multi-degree-of-freedom posture. Additionally, limit holes are set at the ends of the middle frames, and limit pins can be configured according to the actual wall surface conditions to restrict the relative twisting angles of the connection frame in the front and back, ensuring the stability of the robot's structure. The spray rod cleaning system is installed on the front support plate of the connecting frame. Firstly, the base controller is fixed, and the entire spray rod base is supported in the middle, including the rotating base and the pitching base. The lower portion of the pitching base is firmly affixed to the rotating base, while the upper section secures the spray rod in position via clamping elements. The base can be manually manipulated and locked for adjusting the pitching angle, guaranteeing that the spray rod angle remains stable during cleaning operations.

2.3. Analysis of the Wall Adaptability of the Robot

In accordance with the design requirements of the cleaning robot, the tracked mobile mechanism is required to adapt to the arc surface with a radius greater than 2000 mm in both lateral and longitudinal movements. According to the structural principle, during lateral

operation, the track can be freely adjusted within the pitching angle range, and the extreme position is determined by the geometric position. Compared with other wall-climbing robots that employ force closure on curved surfaces [22–24], the adjustment mechanism is simpler. As shown in Figure 4, when the robot is crawling laterally on the curved surface, the mobile mechanism adapts to the convex and concave surfaces by automatically tilting an angle. According to the geometric size relationship, the tilting angle ϕ is as follows:

$$\phi = \arcsin\frac{0.5L_1 + 0.5L_2 + c}{R + r + d_1 + d_2} \tag{1}$$

where R is the radius of the panel, mm; r is the radius of the track wheel, mm; d_1 is the thickness of the track, mm; d_2 is the thickness of the magnet, mm; L_1 is the width of the robot connection frame, mm; L_2 is the outer width of the mobile mechanism, mm; and c is the installation clearance between the mobile mechanism and the connection frame, mm.

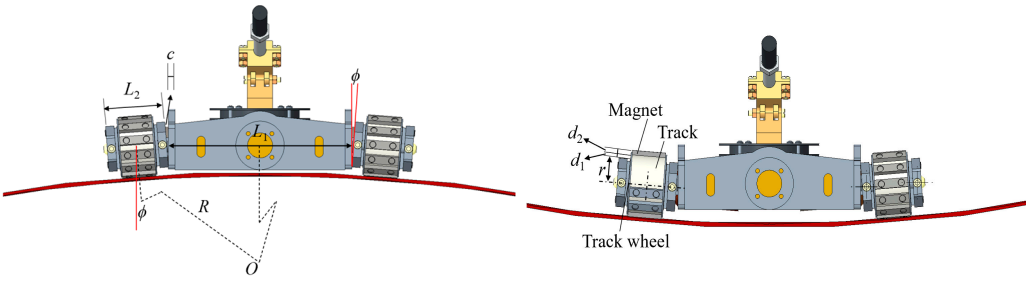


Figure 4. Transverse crawling on the curved surface.

When the robot is crawling longitudinally on the arc surface, because the magnet is fixed on the outside of the track in the adsorption mode and the track has certain elasticity, the track will automatically fit along the arc surface to a certain extent under the action of magnetic force. Meanwhile, for the robot with the same load capacity, it adopts a front-and-rear segmented structure, which enables the track to have more contact with the arc surface, thereby reducing the gap between the front and rear ends of the track and the wall surface and enhancing the stability and adaptability of the crawling. As shown in Figure 5, taking the track status of the robot before and after crawling on a convex surface as an example, considering the small radius of the track wheelbase relative to the curved surface and the relatively small elastic deformation of the track adapting to the convex surface shape, the arc ground length can be equivalent to the track wheelbase. Additionally, by considering the relationship between the spacing of the magnets and the curvature of the arc, the angle α_i through which each magnet rotates can be approximated as

$$\begin{cases} \alpha_i \approx \frac{180L_3}{\pi R(n-1)}\left|\frac{n+1}{2} - i\right| \\ n = \frac{L_3}{2P_b} \end{cases} \tag{2}$$

where L_3 is the track wheelbase (magnetic adhesion ground length), mm; P_b is the track pitch, mm; n is the quantity of single-track ground magnets; and i is the sequence of the ground magnet from the front to the rear, 1, …, n. The turning angle of the magnet varies at different grounding positions. Evidently, the turning angle of the magnet at the end of the track is the greatest; that is, i = 1 or n. Then $\alpha_{i\text{-max}}$ can be expressed as

$$\alpha_{i-\max} = \frac{90L_3}{\pi R} \tag{3}$$

Similarly, the turning angle α'_i through which the rear track magnet follows the curved surface can also be referred to in the form of Equation (2).

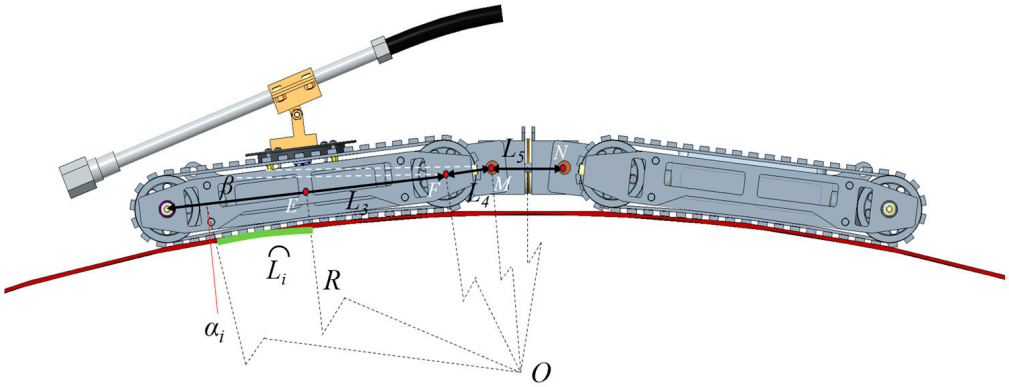


Figure 5. Longitudinal crawling on the curved surface.

The overall attitude adjustment angle β of the tracked crawling mechanism on curved surfaces with different curvature radii can be derived based on the following relationship:

$$\begin{cases} \beta = \pi - \angle FMO - \angle NMO \\ \angle FMO = \arccos\frac{0.5L_3+L_4}{MO} \\ \angle NMO = \arccos\frac{0.5L_5}{MO} \\ MO^2 = EO^2 + (0.5L_3 + L_4)^2 \\ EO^2 = (R + r + d_1 + d_2)^2 - (0.5L_3)^2 \end{cases} \tag{4}$$

where L_4 is the distance between the driven wheel and the hinge position which connected the side frame and the middle frame, mm; and L_5 is the distance between the middle frame and the hinged position formed by the front and rear side frames, mm. The partial structural parameters of the robot are set as follows: r is 30.9 mm, d_1 is 2 mm, d_2 is 5 mm, L_1 is 220 mm, L_2 is 70 mm, L_3 is 300 mm, c is 2 mm, L_5 is 75 mm, L_4 is 50 mm, and P_b is 10 mm. By applying Equations (1)–(4), the variations of ϕ, $\alpha_{i\text{-max}}$, and β, with the change of R, are acquired, as well as the variations of α_i at different magnet positions when R is 2000 mm, with n as 15, as shown in Figure 6.

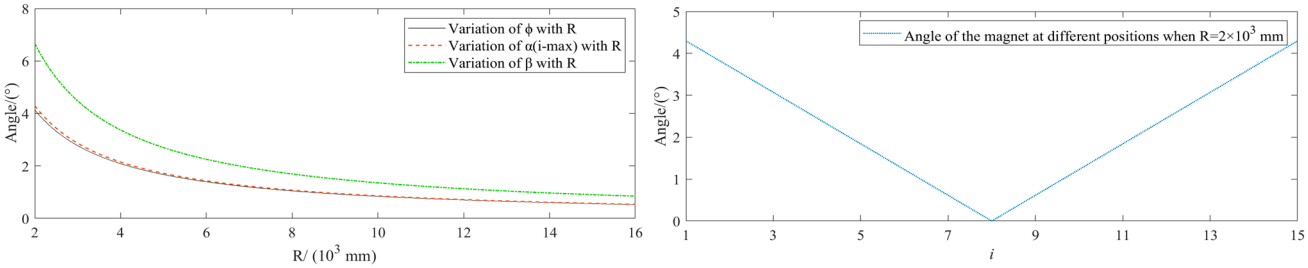


Figure 6. Analysis of the variation of robot angle parameters.

With the increase in R, angles ϕ, $\alpha_{i\text{-max}}$, and β all decrease gradually, and the decreasing range is large first and then small. When R is 2000 mm, ϕ_{max} is approximately 4.1°, $\alpha_{i\text{-max}}$ is approximately 4.3°, and β_{max} is approximately 6.7°. For the same track ground magnet, the maximum angle of the magnets at both ends is about 4.3°.

Furthermore, during oblique crawling or steering on the curved surface, the relative rotation of the middle plates induces the self-adaptive twisting of the front and rear structures, enhancing the adhesion stability of the four tracked mobile mechanisms on surfaces with different curvatures, which is conducive to enhancing the overall crawling adaptability of the cleaning robot, as shown in Figure 7.

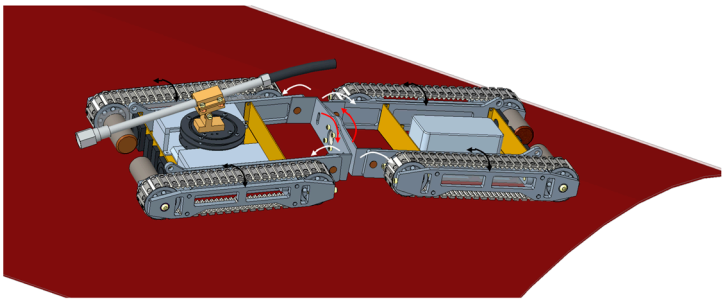


Figure 7. Oblique crawling on the curved surface.

3. Mechanical Analysis

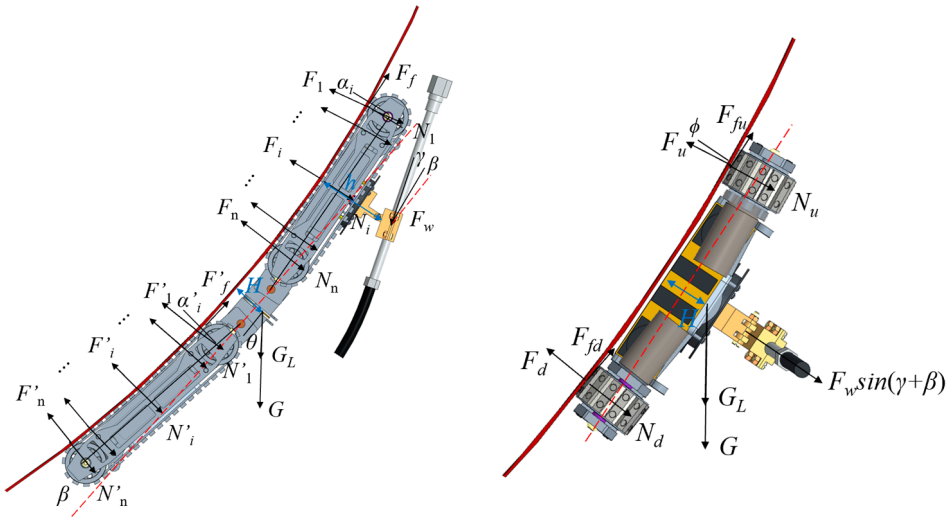
3.1. Instability Analysis

Crawling constitutes a fundamental function of cleaning robots, irrespective of whether the wall is plane or curved. Slipping and tipping represent the principal instability phenomena. In contrast to single-function wall-climbing robots, the water-jet impact reaction force constitutes an additional force in the cleaning robot and varies with alterations in cleaning parameters. When operating on a curved surface, the robot's posture undergoes continuous changes, and the direction of instability also undergoes changes. Based on the results of the adaptability analysis in the preceding section, a static analysis of the cleaning robot in the longitudinal and transverse directions of the curved surface is conducted.

(1) Longitudinal slip analysis. As shown in Figure 8a, a static model for longitudinal slip on a curved surface is established, and the subsequent equation is obtained:

$$\begin{cases} 2\sum_{i=1}^{n}(F_i - N_i)\cos\alpha_i + 2\sum_{i=1}^{n}(F_i' - N_i')\cos\alpha_i' = \dfrac{(G+G_L)\sin\theta + F_w\sin(\gamma+\beta)}{\cos\beta} \\ F_i = F_i' = F_m \end{cases} \tag{5}$$

where F_w is the reaction force of the jet on the spray rod, which is approximately considered as the reverse impact force of the jet [25,26]. It can be expressed as $F_w = 0.745Q\sqrt{P}$, where Q represents the jet flow rate, set as 20 L/min, and P represents the outlet pressure, set as 10 MPa.



(**a**) (**b**)

Figure 8. Static force analysis; (**a**) longitudinal state; (**b**) transverse state.

When the robot does not undergo slipping, the following condition is fulfilled:

$$2(F_f + F'_f) = 2f(\sum_{i=1}^{n} N_i \cos\alpha_j + \sum_{i=1}^{n} N'_i \cos\alpha'_i)\cos\beta \geq (G + G_L)\cos\theta + F_w \cos(\gamma + \beta) \quad (6)$$

where f is the static friction coefficient, which can be set to 0.4 [27–29]. By solving Equations (5) and (6), it is obtained that the magnet adsorption force should meet the following conditions:

$$F_m \geq \frac{(G + G_L)(\cos\theta + f\sin\theta) + fF_w \sin(\gamma + \beta) + F_w \cos(\gamma + \beta)}{2f\cos\beta(\sum_{i=1}^{n} \cos\alpha_i + \sum_{i=1}^{n} \cos\alpha'_i)} \quad (7)$$

(2) Longitudinal tipping analysis.

In the longitudinal posture, the tipping moment is produced under the influence of gravity and the jet reaction force, which necessitates balancing by the anti-tipping moment. In line with the crawling characteristics of the multi-track mechanism, the detachment of the magnets at both ends of the track from the wall serves as the condition for tipping instability [30]. The force on the curved surface is equivalent to the body attitude direction, and the following relationship can be obtained:

$$\begin{aligned} &2(F_1 - N_1)[(2L_3 + 2L_4)\cos\beta + L_5]\cos\alpha_1 \cos\beta + 2(F'_1 - N'_1)\cos\alpha'_1 \cos\beta \cdot L_3 \cos\beta \\ &+2(F_n - N_n)[(L_3 + 2L_4)\cos\beta + L_5]\cos\alpha_n \cos\beta \geq (G + G_L)[(L_3 + L_4)\cos\beta + 0.5L_5]\sin\theta \\ &+(G + G_L)H\cos\theta + F_w[(1.5L_3 + 2L_4)\cos\beta + L_5]\sin(\gamma + \beta) + F_w h\cos(\gamma + \beta) \end{aligned} \quad (8)$$

$$F_m \geq \frac{\begin{array}{l}(G + G_L)[(L_3\cos\beta + L_4\cos\beta + 0.5L_5)\sin\theta + H\cos\theta] + \\ F_w[(1.5L_3\cos\beta + 2L_4\cos\beta + L_5)\sin(\gamma + \beta) + h\cos(\gamma + \beta)]\end{array}}{2[(4L_3 + 4L_4)\cos\beta + 2L_5]\cos\alpha_{1(n)}\cos\beta} \quad (9)$$

(3) Transverse tipping analysis.

When in the transverse posture, the upper track leaves the wall surface as the critical condition for transverse tipping. The force on the curved surface is equivalent to the body attitude direction, and the following relationship can be obtained:

$$\begin{cases} 2(F_u - N_u)(L_1 + L_2 + 2c)\cos\phi \geq (G + G_L)H\cos\theta \\ +[(G + G_L)\sin\theta + F_w \sin(\gamma + \beta)](0.5L_1 + 0.5L_2 + c) \\ F_u = nF_m \end{cases} \quad (10)$$

Then, under the condition of transverse tipping, the magnetic adhesive force is satisfied:

$$F_m \geq \frac{(G + G_L)[(0.5L_1 + 0.5L_2 + c)\sin\theta + H\cos\theta] + F_w(0.5L_1 + 0.5L_2 + c)(\sin\gamma + \beta)}{2n(L_1 + L_2 + 2c)\cos\phi} \quad (11)$$

It is given that G is 170 N, G_L is 50 N, γ is 30°, θ ranges from 0 to 30°, and H and h are measured via a three-dimensional model, with values of 42 mm and 120 mm, respectively. Through substituting into Equations (7), (9), and (11), the required adhesive force in the three crawling states is analyzed, and the variation of the adhesive force with θ is presented in Figure 9. With the increase in θ, the adsorption force of each state gradually increases, and the rate of increase decreases in sequence from the longitudinal tip state, the slipping state, and the transverse tip state. The adhesive force in the longitudinal tip state undergoes the most significant change with θ, and the maximum adhesive force is 19.2 N when θ is 30°. Hence, the minimum adhesive force necessary for the cleaning robot not to experience instability on the wall is no less than 19.2 N. The 40 × 10 × 5 mm magnet is chosen, and the vertical stable adhesive force is approximately 21 N.

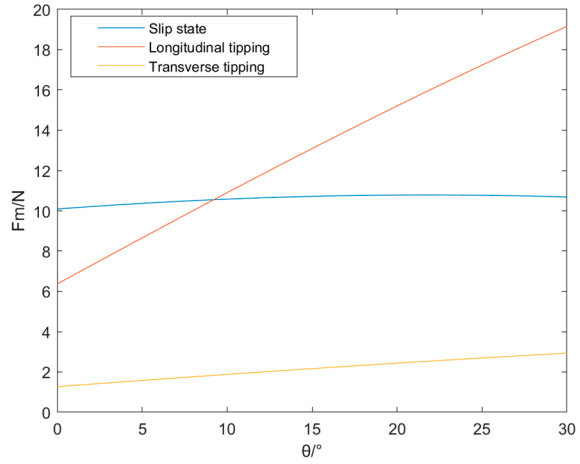


Figure 9. The change of adsorption force with θ in different states.

3.2. Driving Torque Analysis

When the cleaning robot crawls on the panel, the driving torque must guarantee the accomplishment of longitudinal, transverse, and steering movements. In accordance with the cleaning operation principle and for enhancing cleaning operation efficiency, it is stipulated that the robot can conduct cleaning operations while crawling longitudinally or transversely but not during steering. The driving torque of the cleaning robot is provided by four sets of motors, which enable the robot to crawl stably by overcoming the gravitational resistance moment, the jet reaction moment, the friction resistance moment, and the resistance moment formed by the last magnet of the track. Considering that the driving torque required for upward crawling and the steering motion is larger, an analysis is carried out on this object.

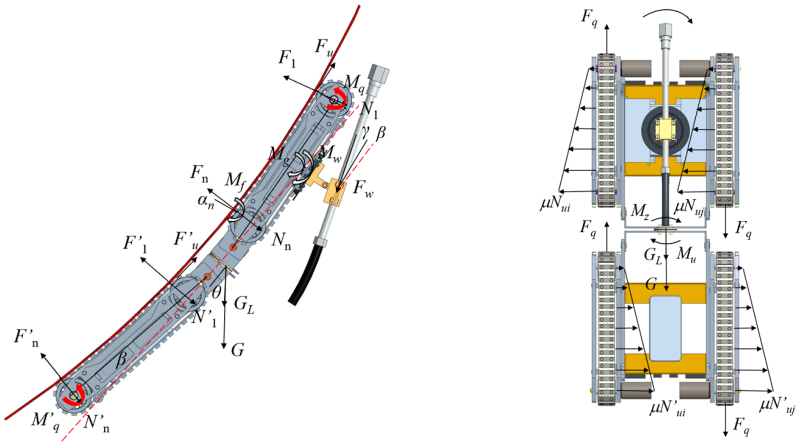
(1) Upward crawling

As shown in Figure 10a, the robot is crawling upward. Because the spray rod is installed on the front track and the front and rear bodies are hinged and connected, no torque is transmitted, so the resistance moment formed by the jet reaction force mainly acts on the front track, which requires the motor-driving torque of the front track to be larger. Considering the resistance moment formed by the last magnet of the track, on the premise of ensuring no slip, the driving torque of the front and side track can be expressed as

$$\begin{cases} M_q \geq M_g + M_w + M_f \\ M_g = \frac{(G+G_L)H\cos\theta}{4} \\ M_w = \frac{F_w h\cos(\gamma+\beta)}{2} \\ M_f = [F_m - \frac{(G+G_L)\sin\theta}{4n\cos\alpha_n} - \frac{F_w\sin(\gamma+\beta)}{2n\cos\alpha_n}]\cdot b \end{cases} \tag{12}$$

where M_q is the driving torque of the front track motor, N·m; M_g is the gravitational resistance moment of the single track, N·m; M_w is the jet resistance moment of the front single track, N·m; M_f is the resistance moment formed by the last magnet of the track, N·m; and b is the distance between the magnetic adhesion force of the last set of magnets and the actual support force, which is taken as 5 mm. Through simplifying Equation (10), the following can be obtained:

$$M_q \geq \frac{(G+G_L)}{4}(H\cos\theta - \frac{b\sin\theta}{n\cos\alpha_n}) + \frac{F_w}{2}[h\cos(\gamma+\beta) - \frac{b\sin(\gamma+\beta)}{n\cos\alpha_n}] + F_m b \tag{13}$$



(**a**) (**b**)

Figure 10. Driving torque analysis; (**a**) upward crawling; (**b**) steering.

It can be seen that with the increase in θ, M_q gradually decreases; when θ is 0, there is the maximum driving torque; then the robot can be considered to crawl upward on the vertical panel, and the following relationship is obtained:

$$M_q \geq \frac{(G+G_L)H}{4} + \frac{F_w}{2}[h\cos(\gamma+\beta) - \frac{b\sin(\gamma+\beta)}{n}] + F_m b \tag{14}$$

(2) Steering

As shown in Figure 10b, the steering of the crawler wall-climbing robot on the wall is mainly realized through the reverse drive of the crawler on both sides. The steering torque M_z generated by the crawler on both sides overcomes the resistance moment M_u caused by the sliding friction force of the magnet on the track. Assuming that the wall surface is a straight plane, then

$$\begin{cases} M_z \geq M_u \\ M_z = 2F_q(L_1+L_2+2c) \\ F_q = \frac{M_q}{r} \\ M_u = \sum\limits_{i=1}^{n}(N_{ui}+N'_{ui})\mu l_i + \sum\limits_{j=1}^{n}(N_{uj}+N'_{uj})\mu l_j \end{cases} \tag{15}$$

where N_{ui}, N'_{ui}, N_{uj}, and N'_{uj} are the support forces exerted by the wall on the four sets of magnets during the track's steering process at different positions, N; l_i and l_j are the distances of the i-th or j-th magnet on the left or right track from the center of the track, mm; and μ is the coefficient of sliding friction, which can be set to 0.3. Grounded on the overall structural relationship and the premise that no cleaning operation is carried out during the steering process, the following relationship holds:

$$N_{ui(j)} = N'_{ui(j)} = F_m - \frac{(G+G_L)\sin\theta}{4n} \pm \frac{(G+G_L)H}{4l_{i(j)}} \tag{16}$$

In this equation, when $i(j) \leq 0.5n$, the symbol takes the value of "-", and when $i(j) > 0.5n$, the symbol takes the value of "+". By consolidating Equations (13) and (14), the following can be obtained:

$$M_q \geq \frac{\mu r[4F_m n - (G+G_L)\sin\theta]}{2(L_1+L_2+2c)n} \sum_{i(j)=1}^{n} l_{i(j)} \tag{17}$$

According to Equations (14) and (17), the motor-driving torque should be greater than 3.5 N·m. The drive motor is a custom-made M3508 gear motor.

4. Control System

The cleaning robot works on gate panels with a wide range of widths and heights, so it is often far from being under direct human control. The robot adopts wireless remote control mode and realizes efficient panel cleaning by rationally arranging the positions of cleaning robots, pumps, cables, etc. The above sections carry out the mechanical design and mechanical analysis of the robot, and determine the robot crawling scheme, the water-jet spray rod adjustment mechanism scheme, and the crawling driving torque in different states, which can be used as the design basis for the remote control system. The remote control system mainly controls the crawling action of the robot on the plane and curved panels, and the reciprocating swing action of the water-jet spray rod. In addition, the occurrence of the water jet is realized by manually operating the pump set. According to the above control operation content, this section carries out the composition design of the control system and analyzes the coordination relationship between the swing speed of the spray rod and the crawling speed of the robot so as to ensure the continuous cleaning of the panel and avoid the omission of the cleaning position.

4.1. System Design and Composition

Remote control system design should meet the needs of the actual operation of the function while being easy to understand and operate. It can be composed of the following three parts: robot crawling control, spray rod control, and water-jet control. In light of the structure and control method of the robot, the crawling and spray rod action are remote controlled by the handle, while the water jet control is carried out by a wired ground control. The specific composition of the control system is shown in Figure 11.

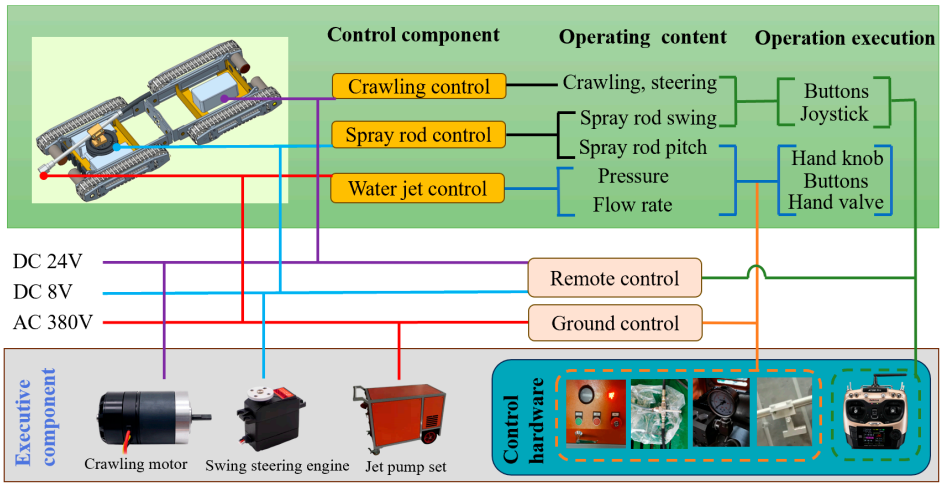


Figure 11. The control system composition of the cleaning robot.

(1) Robot crawling control. By changing the direction of the joystick on the remote control handle, the cleaning robot can be controlled to move forward, backward, and steer so that it can move flexibly on the panel. The remote controller uses the AT9S Pro transmitter to transmit control information stably to the R9DS receiver located at the rear of the robot within 100 m of the ground without obstruction. Four groups of crawling motors cooperate to complete the stable operation of the robot and adjust the speed of the motor according to the PWM signal through the electronic governor to achieve crawling and steering actions at different speeds. The M3508 motor, which acts as a crawling actuator, has a variety of built-in sensors that can automatically detect high temperatures, broken wires, and other anomalies and issue alerts promptly. The position sensor can accurately feed back the position of the motor rotor, and its

own memory chip can automatically record the calibration parameters of the sensor, eliminating the cumbersome calibration process. The crawling drive motor operates at 24 V. To satisfy the long-term crawling operation requirements of the cleaning robot, the power supply adopts a ground energy station with a capacity of 40 Ah.

(2) Spray rod control. According to the mechanical structure design, the spray rod needs to be able to swing left and right in the cleaning operation to expand the cleaning operation range, and the pitch angle of the spray rod is also a controlled parameter, but because the pitch angle is often fixed in the actual operation, the control of the spray rod adopts two modes. The reciprocating swing is a continuous action, so the rotating base is designed and set in the front of the robot, and the swing operation is realized by the remote control of the steering engine. The speed of the steering engine can be set according to the robot crawling speed, and its working voltage is 8 V. For the pitch angle of the spray rod, in order to reduce the load of the robot and the complexity of the structure, the ground control is used to clamp the spray rod and fix the angle through the hand knob. At the same time, in the cleaning operation, the relatively fixed structure avoids the angle deviation of the spray rod due to the water-jet reaction force so as to ensure the same cleaning direction.

(3) Water-jet control. The control of the water jet is mainly the operation of the ground pump set. The drive voltage of the pump set is 380 V, and a water jet with a maximum pressure of 10 MPa can be provided, which meets the requirements of mechanical analysis. The pressure of the jet is controlled by the pressure regulator, which can be adjusted by turning the knob to change the pressure magnitude, and the pressure gauge indicates the pressure. The flow rate and the switching of the cleaning operation can be controlled by a three-way valve, and the cleaning operation can be selected when the pump set is activated.

The above three parts of control ensure that the cleaning robot completes the cleaning operation on the panel, and the cleaning parameters can be adjusted according to different attachment types. In addition, the hardware control system also includes the control board, electronic speed controller, receiver, cables, and heat sink.

4.2. Coordination Analysis of Cleaning and Crawling Speed

To guarantee the efficiency of the cleaning operation, the cleaning robot is expected to possess the capability of cleaning while crawling. Considering that the gate panel typically has a width-to-height ratio greater than one, the actual cleaning operation begins with transverse cleaning from the top of the panel by remote control of the robot. The robot crawls transversely for cleaning until reaching the end, then steers downward and continues the transverse cleaning. In such a manner, continuous operation is executed and forms a clean surface along the robot's crawling direction until the entire panel is cleaned, as shown in Figure 12.

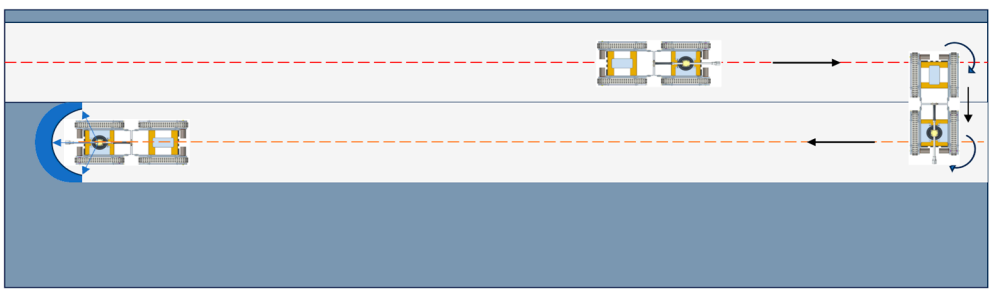


Figure 12. Cleaning operation mode.

During cleaning operations, to prevent any omission of cleaning positions on the panel, the left and right swing amplitude and frequency of the spray rod should match the crawling speed of the robot. Assuming that the area swept by the water jet can quickly

clean the dirty surface, that is, the robot always crawls forward at a stable speed without stopping, the theoretical trajectory formed by the swing of the spray rod is shown in the white center line in Figure 13. Additionally, S' is the distance between the left and right swing boundaries of the nozzle on the spray rod, m; and S is the distance between the two sides of the effective cleaning range, m. Since the jet rod swings to form a curved jet surface, S is always greater than S', and S' is greater than the robot contour width.

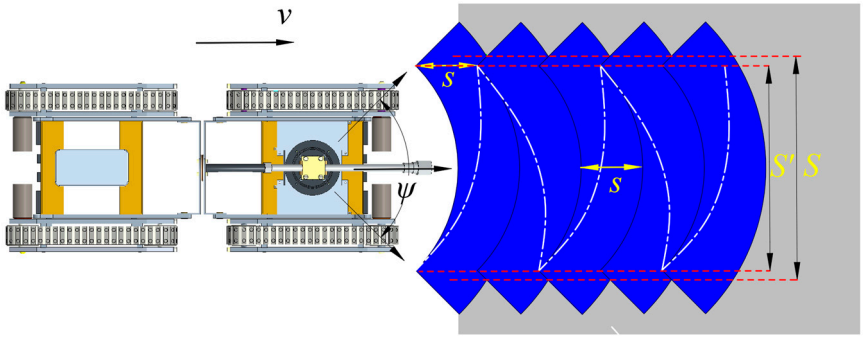


Figure 13. Schematic diagram of the scope of robot cleaning operations.

Due to the fact that there exists a certain impact extension at the contact point between the jet stream and the panel, the forward extension distance is regarded as the criterion and designated as s, m. When the crawling distance of the robot is s, the spray rod needs to complete a one-way swing, and the swing angle is set as ϕ; then the following relationship exists:

$$\frac{s}{v} = \frac{\varphi\pi}{180\omega} \tag{18}$$

where v is the crawling speed of the cleaning robot, m/s; and ω is the angular speed of the spray rod swing, rad/s. Set the swing angle of the spray rod to 90° and the swing time to 1 s. According to the design requirements, when v is greater than 0.05 m/s, in order to ensure an adequate water-jet cleaning range, the ω should be greater than 1.57 rad/s. Therefore, PWM steering engine is used.

5. Experimentation

Based on the above design and analysis process of the crawling mechanism, cleaning mechanism, and control system, a multi-degree-of-freedom wall-climbing cleaning robot prototype with high adaptability to the wall surface was developed for water-jet cleaning of steel gate panels. Its main technical parameters are shown in Table 1.

Table 1. Principal technical parameters of the cleaning robot.

Parameter	Value
Dimensions	850 × 315 × 130 mm
Weight	16.8 kg
Adaptive radius of curvature	≥2000 mm
Spray rod angle	≤30°
Nozzle diameter	2 mm
Signal type	PWM
Main operating voltage	24 V

With reference to the actual scene of the robot cleaning operation (Figure 2), the experiment was set up in the room. According to the mechanical design and the control system design, a planar panel with a width of 2000 mm and a height of 1800 mm, and a curved panel with a radius of 2000 mm are constructed. The robot cleaning system includes the robot body, power source, pump set, and other safety protection facilities. The performance test scene is shown in Figure 14.

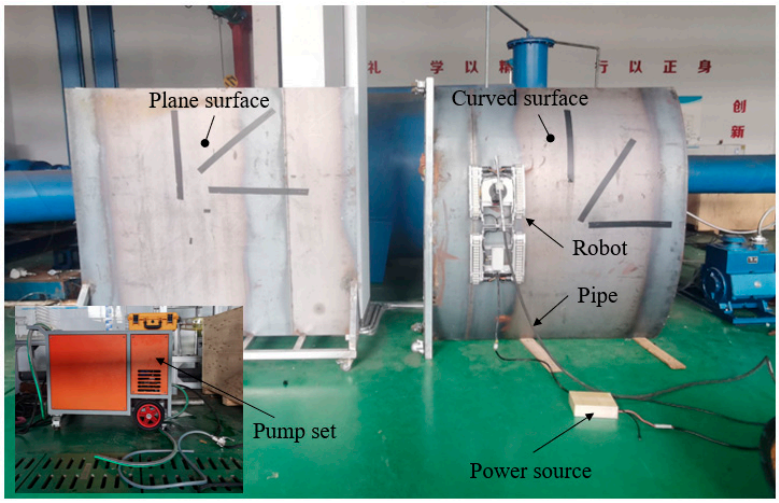


Figure 14. Performance testing scene.

The main performance of the cleaning robot is crawling and its cleaning effect. In the test scene, the two parts of the test were carried out, respectively. The test principle and basic parameters refer to the mechanical design and mechanical analysis, such as the maximum load of 5 kg, a crawling speed greater than 0.05 m/s, the adaptability of split structure combined with the body swing and torsion mechanism to the variable curvature surface and the cleaning test of silt and shellfish, while verifying the stability of the robot during the water-jet cleaning process.

5.1. Crawling Performance Test

Better crawling performance of the robot is the basis for the smooth completion of the entire cleaning operation. Different from wall-climbing robots with other functions, the impact generated by water-jet cleaning panels brings an obvious extra load to the crawling process, so the carrying capacity and stability of the robot are required to be higher. According to mechanical analysis, the robot can stably adsorb and crawl on the panel within a load of 5 kg. In order to verify the theoretical results, the static stability and crawling speed on the plane panel and curved panel are tested, respectively. For the convenience of testing, three groups of loads of 1 kg, 3 kg, and 5 kg were set. Considering that the cleaning pipe connected with the spray rod is suspended, it will not generate additional load on the robot, so in order to facilitate the test, the cleaning pipe is not equipped.

(1) Static stability. In the static state, observe whether the robot has obvious slipping or tipping instability, as shown in Figure 15. The test time is set to 15 min. The results show that under the condition of a load less than 5 kg, the robot can stably adsorb on both the plane and curved surface, and no obvious instability state is observed, which proves that the cleaning robot has good static stability, and the mechanical analysis results of magnetic adsorption force are reasonable.



Figure 15. Static performance test of the robot under load.

(2) Crawling speed. The performance tests of the robot under different crawling conditions and different loads were carried out on the plane and the curved surface,

respectively. According to the structural size of the steel plate, the longitudinal crawling distance was set to be 0.6 m and 0.5 m, the transverse climbing distance was set to be 0.7 m and 0.6 m, and the oblique climbing distance was both set to be 0.7 m. In order to obtain more accurate crawling-speed results and reduce errors, the robot is asked to crawl a certain distance before recording so that the speed reaches a stable value. The crawling time under different loads is recorded, as shown in Table 2. Obviously, no matter what the crawling state, the crawling time also increases with the increase in the load. In each crawling state, the robot can always maintain stable adsorption without instability, which also shows that the design result of magnetic adsorption force is reasonable. The test process is shown in Figures 16 and 17.

Table 2. Crawl time under different loads.

Wall Condition	Longitudinal Crawling			Transverse Crawling			Oblique Crawling		
	Load /(kg)	Distance /(m)	Time /(s)	Load /(kg)	Distance /(m)	Time /(s)	Load /(kg)	Distance /(m)	Time /(s)
Plane surface	0	0.6	5.8	0	0.7	6.6	0	0.7	6.7
	1	0.6	6.6	1	0.7	6.8	1	0.7	7.1
	3	0.6	6.8	3	0.7	7.2	3	0.7	7.5
	5	0.6	7.4	5	0.7	8.0	5	0.7	8.1
Curved surface	0	0.5	5.5	0	0.6	5.7	0	0.7	9.8
	1	0.5	5.8	1	0.6	5.9	1	0.7	10.7
	3	0.5	6.1	3	0.6	6.1	3	0.7	12.5
	5	0.5	7.1	5	0.6	6.9	5	0.7	13.4

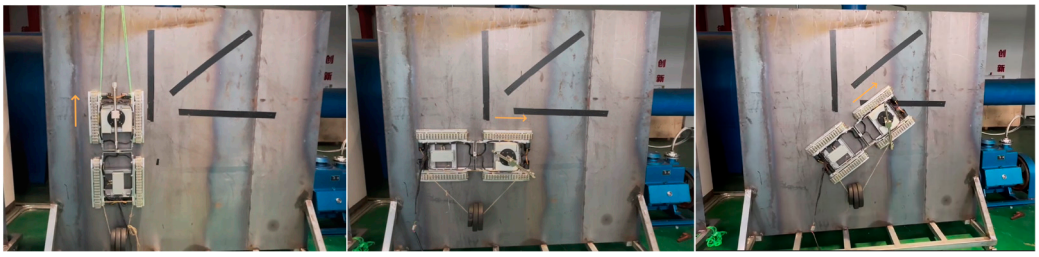


Figure 16. Crawling-speed test on the plane surface.



Figure 17. Crawling-speed test on the curved surface.

According to the recorded parameters, the speed of each crawling test was obtained and analyzed, as shown in Figure 18. With the increase in the load, the speed of each crawling state decreases gradually. Under the same load, no matter what kind of attitude, the crawling speed of the curved surface is slower than that of the plane surface, and in the transverse crawling, the speeds under the two kinds of surface are the closest (Figure 18b), while the speed difference is the most obvious in the oblique crawling (Figure 18c). Under the same wall condition and different crawling posture, the transverse crawling speed is always the largest. For the plane surface, the longitudinal upward crawling speed is slightly less than the oblique crawling speed, but for the oblique upward crawling speed of

the curved surface, because the robot is always adjusting its posture, the crawling speed is slower than the longitudinal upward crawling speed. When the robot is unloaded, the maximum crawling speed is 0.107 m/s. At the maximum load, the crawling speed is between 0.052 m/s and 0.088 m/s. It can be seen that the crawling speed of the robot under different loads and on different panels is greater than 0.05 m/s, which meets the design requirements and verifies that the motor selected based on the driving-torque analysis results is reasonable and effective.

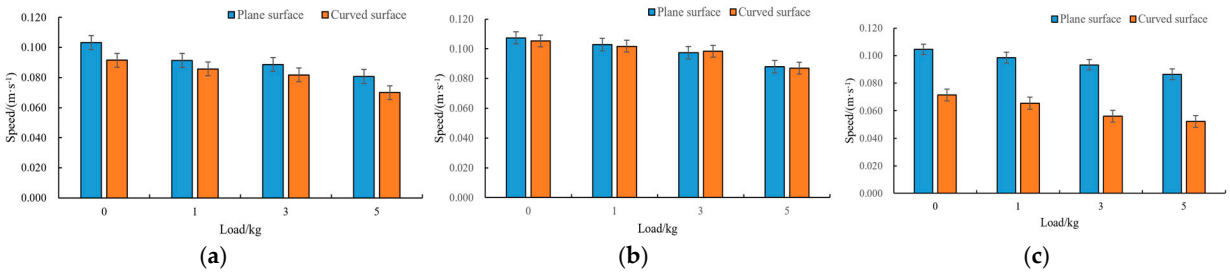


Figure 18. Analysis of crawling-speed test results; (**a**) longitudinal crawling; (**b**); transverse crawling; (**c**) oblique crawling.

(3) Curved surface adaptation ability. The unique adjustment mechanism enables the robot to adapt to different surface working conditions. As shown in Figure 19a,b, the robot can maintain stable adherence to the wall surface in both the transverse and longitudinal directions by adjusting the swing of the crawling mechanism and the twisting of the front and rear frames. During oblique crawling, the front and rear frames have obvious twisting, marked by the red line in Figure 19c, which makes the front and rear bodies more compliant with the curvature changes of different track adsorption positions. It is obvious that the magnets on the track are firmly adsorbed on the curved surface, as shown in Figure 19d, indicating that the designed robot structure has good wall adaptability.

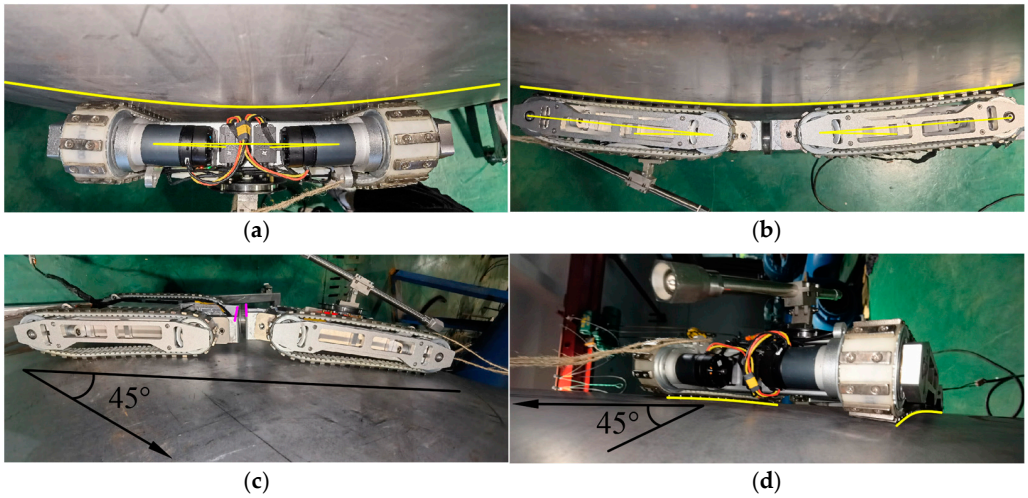


Figure 19. Curved surface adjustment ability test; (**a**) adaptive adsorption during transverse crawling; (**b**) adaptive adsorption during longitudinal crawling; (**c**) obvious twisting during oblique crawling; (**d**) adaptive adsorption during oblique crawling.

5.2. Cleaning Performance Test

It can be concluded from the previous analysis that the attachments to the panel are mainly silt, secretions of aquatic plants, and shellfish. It was found that the adhesions of silt and secretions were close to each other and relatively small, while the adhesion of shellfish was relatively large. Therefore, in order to verify the cleaning performance of the

cleaning robot, silt and shellfish are selected as the cleaning objects, and the linear cleaning characteristics and swinging cleaning characteristics of the water jet were tested. According to the proposed cleaning operation mode, the test is completed in the transverse crawling state of the robot. At the same time, three groups of angles of 30°, 20°, and 10° are set according to the design of the spray rod angle less than 30° adopted in the mechanical analysis. The jet pressure is 2 MPa.

(1) Silt cleaning. First, the test of water-jet straight-line cleaning of silt was carried out, as shown in Figure 20a,b. At a spray rod angle of 30°, the water jet impacted the silt surface near the front end of the robot. The cleaning time was set at 5 s, and the silt surface was cleaned out to an obvious area. In the cleaning process, the robot structure is stable, and the magnet is not detached from the wall, indicating that the adsorption force of the robot meets the reverse impact force of the jet, and no obvious slip phenomenon occurs.

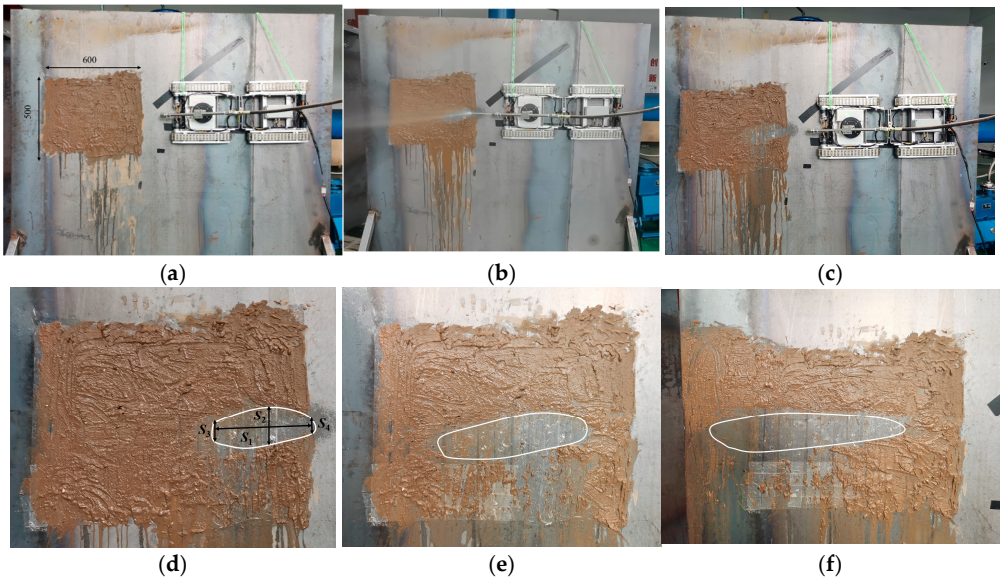


Figure 20. Straight-line cleaning silt test; (**a**) cleaning scenario; (**b**) cleaning process; (**c**) cleaning complete; (**d**) 30°; (**e**) 20°; (**f**) 10°.

Under the same cleaning duration, the cleaning effect of the spray rod on the panel silt at different angles is shown in Figure 20c–e, forming an obvious cleaning surface. In the cleaning process, the robot structure is stable, and the magnet is not detached from the panel, indicating that the adsorption force of the robot meets the reverse impact force of the jet, and no obvious slip phenomenon occurs. This proves that it is reasonable to take the jet reaction and spray rod angle as the stability factors affecting the robot cleaning operation in mechanical analysis. The range of the cleaning surface obtained is analyzed, and four parameters are defined, as shown in Figure 21, where S_1 and S_2 are depth and maximum width of the jet surface, respectively, mm; and S_3 and S_4 are the jet width at the head and tail of the jet surface 10 mm from the boundary point, respectively, mm. The results show that as the spray rod angle decreases, S_1 increases significantly, and the cleaning area becomes flatter. S_2 and S_3 show a decreasing trend, but the difference is small, while S_4 is close, and the change is not obvious.

With the increase in jet washing time, the water mist formed by jet diffusion continuously soaks the distant silt. Due to the small adhesion of the silt on the panel, the soaked silt is more likely to fall, thus increasing the scope of the cleaning surface. Considering the size of the silt surface arranged, the test takes the spray rod at 30° as an example, and the swing angle is set at 90°, as shown in Figure 22. The spray rod completed the swinging cleaning operation from right to left, and the radiant surface of the jet covered almost all

the silt in the flushing direction. The cleaning surface directly formed by the flushing was a fan-shaped area, and the measured depth marked S_5 was about 225 mm.

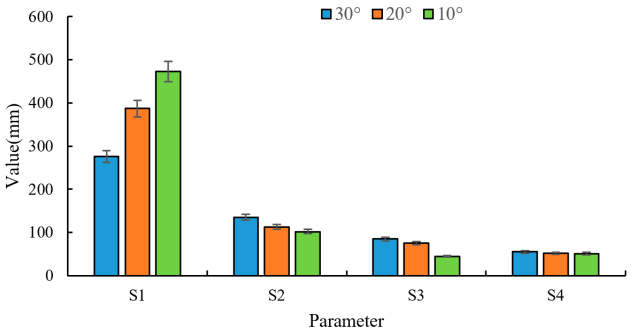


Figure 21. Parameters of the range of silt cleaning surface at different spray rod angles.

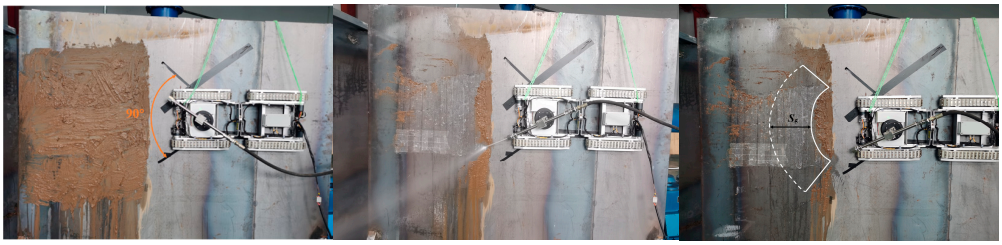


Figure 22. Swinging cleaning silt test.

(2) Shellfish cleaning. The test of water-jet straight-line cleaning of shellfish was carried out, and shellfish were adhered to the wall to simulate the adsorption effect according to Ref. [7]. As shown in Figure 23a,b, when the spray rod angle is less than 30°, the water jet washes the shellfish surface near the front end of the robot. The cleaning time is 5 s, and the shellfish surface is cleaned out to an obvious area. During shellfish cleaning, the robot structure is stable, and no obvious instability occurs. Different from the silt surface, the attachment of shellfish is discrete, which makes the cleaning effect of jet diffusion on the surrounding shellfish weaker than that of silt cleaning except for the central jet area, so the cleaning area formed is also smaller.

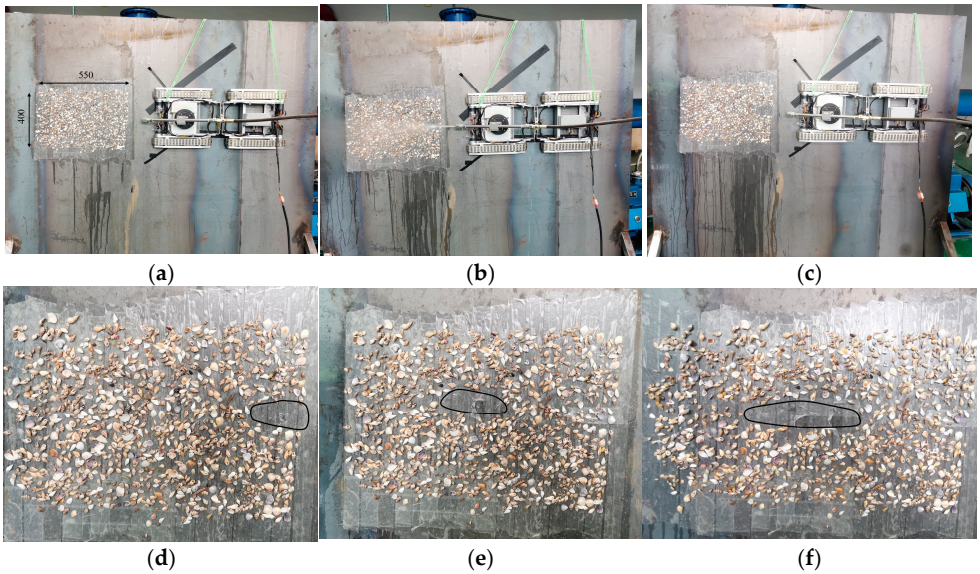


Figure 23. Straight-line cleaning shellfish test: (**a**) cleaning scenario; (**b**) cleaning process; (**c**) cleaning complete; (**d**) 30°; (**e**) 20°; (**f**) 10°.

Under the same cleaning duration, the cleaning effect of the spray rod on the panel shellfish at different angles is shown in Figure 23c–e, forming an obvious cleaning surface. The results (Figure 24) show that S_1 increases gradually with the decrease of the spray rod angle, but the increase of S_1 is small when compared with 30° and 20°, and the increase is obvious when compared with 20° and 10°. The formed cleaning area is relatively flat, and S_2 is smaller than the operation when cleaning silt. Because of the discrete distribution of shellfish, the parameters of S_3 and S_4 are not obvious and relatively close.

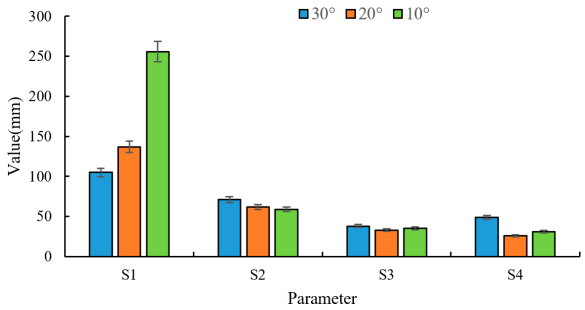


Figure 24. Parameters of the range of shellfish cleaning surface at different spray rod angles.

The spray rod swinging cleaning test was also carried out. As the adhesion of shellfish is greater than that of silt, with the increase in jet washing time, the water mist formed by jet diffusion does not have a tendency to increase during the swinging as when cleaning the silt surface. The spray rod angles of 30°, 20°, and 10° were tested, respectively, as shown in Figure 25. The spray rod completes the swinging cleaning operation from right to left, forming a more obvious cleaning area. As the angle of the spray rod decreases, the width of the cleaning surface increases obviously, but the depth does not increase significantly. The measured depths of the swinging cleaning operation under different spray rod angles are 76 mm, 98 mm, and 136 mm, respectively.

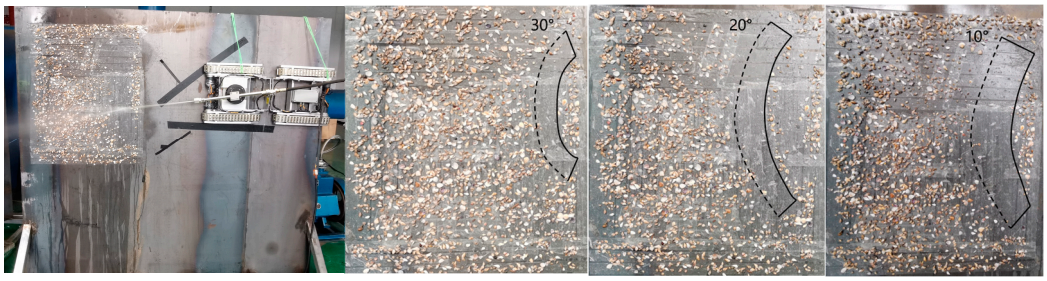


Figure 25. Swinging cleaning shellfish test.

6. Conclusions

Based on stable crawling and reliable wall adaptability, a water-jet cleaning robot was designed for cleaning steel gate panels in river and ocean engineering. Considering the requirements of the plane surface and the curved surface on the crawling ability of the robot, a multi-body robot structure was proposed, which can realize the swing of the moving mechanism and the torsion of the front and rear bodies. The adaptability of the wall surface was analyzed, and the required structural parameters were obtained. Based on this, instability analysis and driving force analysis of the cleaning robot were carried out, so that it has the adaptability of crawling on the panel with a radius greater than 2000 mm, including longitudinal, transverse, oblique, and steering crawling.

A cleaning mechanism which can swing reciprocally and adjust the angle of the spray rod was designed, and coordination analysis of the crawling and cleaning speed was carried out to improve the cleaning effect and efficiency. The robot control system was constructed and the system composition was designed to realize the manual remote cleaning control of the steel gate panel.

The performance tests show that the developed split four-track water-jet cleaning robot can adapt to the plane and curved panel to crawl safely and stably and adapt to the function of the adjusting mechanism to meet the requirements. When the maximum load is 5 kg, the crawling speed is 0.052–0.088 m/s. For the main panel attachments such as silt and shellfish, the spray rod angle is less than 30° to have a better cleaning effect. Compared with the silt surface, the cleaning area formed by the discrete shellfish attachment surface is smaller. The smaller the adjustment angle of the spray rod, the greater the cleaning depth; the continuous cleaning process of the spray rod swing is reliable, and the adsorption is stable. It is indicated that the cleaning robot can meet the design requirements, and the testing method of prototype crawling and cleaning performance based on the mechanical design and mechanical analysis is reasonable. The design and application of a split four-track water-jet cleaning robot is beneficial to the development of the cleaning and maintenance of steel gate panels in river and sea engineering.

In future work, we will carry out mechanical structure optimization of the split four-track cleaning robot and the water-jet cleaning mechanism research further. On the basis of satisfying the basic operation ability, research related to robot automatic control design and path planning to improve the level of intelligent control is the next direction.

Author Contributions: Conceptualization, Z.D. and G.F.; methodology, Z.D.; software, J.C.; validation, Z.D., G.S. and J.Z.; investigation, G.S.; resources, H.Q.; data curation, J.C.; writing—original draft preparation, Z.D.; writing—review and editing, Z.D. and G.F.; visualization, J.Z. All authors have read and agreed to the published version of the manuscript.

Funding: This research was funded by the Basic Public Welfare Research Project of Zhejiang Province (Grant No. LGG22F030024), the Key R&D Program of Zhejiang Province (Grant No. 2022C02035) and the General Scientific Research Project of Zhejiang Education Department (Grant No. Y202147438).

Data Availability Statement: All data are presented in this article in the form of figures and tables.

Conflicts of Interest: The research was conducted in the absence of any commercial or financial relationships that could be construed as a potential conflict of interest.

References

1. Basack, S.; Goswami, G.; Deka, P.; Borah, P.; Mastorakis, N. Analysis and control of flow parameters through sluice gate in dam. *Int. J. Mech.* **2020**, *14*, 22–27.
2. Liang, X.; Zhang, Q.; Huang, W.; Dau, Z.; Cai, J. Experimental and numerical study on static performance of ship lock sector gates. *J. Constr. Steel Res.* **2024**, *222*, 108977. [CrossRef]
3. Luo, Y.; Huang, C.; Guan, Y. Selection and design of service gate of Shuangqiao hub's ship lock. *Port Waterw. Eng.* **2023**, *04*, 143–148.
4. Wang, P.; Su, C.; Jing, S.; Yuan, W.; Wu, Z. Reservoir Flood Control Operation Considering Spillway Gate Scheduling. *Water Resour. Hydropower Eng.* **2024**, *55*, 104–115.
5. Dong, X.; Li, Y.; Yu, Z. The Method of Diagnosis for Corrosion Hydraulic Gate Based on Strain Mode and Frequency. *IOP Conf. Ser. Earth Environ. Sci.* **2019**, *304*, 032049. [CrossRef]
6. Jiang, C.; Fan, K.; Luo, X.; Qian, L. The Corrosion Evaluation Methodology of the Lock Gate. *Adv. Mater. Res.* **2014**, *937*, 105–108. [CrossRef]
7. Huang, S.; Huang, J.; He, K. Research on Erosion Effect of Various Submerged Cavitating Jet Nozzles and Design of Self-Rotating Cleaning Device. *Appl. Sci.* **2024**, *14*, 1433. [CrossRef]
8. Wei, K.; Zhang, Z.; Zhou, Z. Design of a new composite underwater hull cleaning robot. *J. Sea Res.* **2024**, *198*, 102488. [CrossRef]
9. Orozco-Magdaleno, C.E.; Castillo-Castaneda, E.; Carbone, G. Design of a Service Robot for High-Pressure Cleaning. In *The International Conference of IFToMM ITALY*; Springer International Publishing: Cham, Switzerland, 2022.
10. Yan, H.; Niu, H.; Chang, Q.; Zhao, P.; He, B. Study on Dynamic Characteristics of Pipeline Jet Cleaning Robot. *Actuators* **2024**, *13*, 49. [CrossRef]
11. Feng, G.; Li, W.; Li, Z.; He, Z. Development of a Wheeled and Wall-pressing Type In-Pipe Robot for Water Pipelines Cleaning and its Traveling Capability. *Mechanika* **2020**, *26*, 134–145. [CrossRef]
12. Yang, P.; Jia, J.; Sun, L.; Zhang, M.; Lv, D. Design and Analysis of a Push Shovel-Type Hull-Cleaning Wall-Climbing Robot. *J. Field Robot.* **2024**, 1–17. [CrossRef]
13. Liao, S.; Deng, S.; Zhao, H.; Guan, J.; Yao, L. Development of Intelligent Cleaning and Rust Removal Machine for Oil Storage Tank Based on Cavitation Water Jet. *Contemp. Chem. Ind.* **2019**, *48*, 2107–2111.

14. Yi, Z.; Gong, Y.; Wang, Z.; Wang, X. Dynamic Modeling and Analysis on a New Type Wall-climbing Robot for Ship Wall Rust Removal. *J. Mech. Eng.* **2010**, *46*, 23–30. [CrossRef]
15. Zhang, J.; Zhang, Q.; Zhang, X. Control System Design of Wheeled Permanent Magnet Wall-climbing Descaling Robot. *Sci. Technol. Eng.* **2018**, *18*, 217–221.
16. Hu, S.; Peng, R.; He, K.; Li, J.; Cai, J.; Zhou, W. Structural design and magnetic force analysis of a new crawler-type permanent magnetic adsorption wall—Climbing. In Proceedings of the IEEE International Conference on Information and Automation, Macau SAR, China, 18–20 July 2017.
17. Zhang, Z.; Lan, J.; Fan, F.; Zhi, X. Selection of New Type Radial Steel Gate and Analysis of Static and Dynamic Characteristics. *Int. J. Steel Struct.* **2021**, *21*, 1630–1643. [CrossRef]
18. Zhang, B.; Jing, X. Theoretical analysis and simulation calculation of hydrodynamic pressure pulsation efect and fow induced vibration response of radial gate structure. *Sci. Rep.* **2022**, *12*, 21932. [CrossRef] [PubMed]
19. Chao, X.; Wang, Z.; Zhang, H.; Li, H.; Li, D. Investigation on mode-coupling parametric vibrations and instability of spillway radial gates under hydrodynamic excitation. *Appl. Math. Model.* **2022**, *106*, 715–741.
20. Lu, Y.; Liu, Y.; Zhang, D.; Cao, Z.; Fu, X. Chaotic Characteristic Analysis of Spillway Radial Gate Vibration under Discharge Excitation. *Appl. Sci.* **2023**, *14*, 99. [CrossRef]
21. Han, Y.; Zhang, X.; Cai, K.; Chai, X.; Li, J.; Wang, Z. Numerical Optimization of the Dendritic Arm of a Radial Gate Based on Stability and Light Weight. *Sustainability* **2022**, *14*, 16507. [CrossRef]
22. Jiang, Z.; Ma, Z.; Ju, Z.; Wang, D.; Xu, Y. Design and analysis of a wall-climbing robot for passive adaptive movement on variable-curvature metal facades. *J. Field Robot.* **2022**, *40*, 94–109. [CrossRef]
23. Hu, J.; Han, X.; Tao, Y.; Feng, S. A magnetic crawler wall-climbing robot with capacity of high payload on the convex surface. *Robot. Auton. Syst.* **2022**, *148*, 103907. [CrossRef]
24. Jiang, Z.; Zhao, Z.; Chen, B.; Li, Y.; Zhao, Y.; Xu, Y. Design and analysis of a passive adaptive wall-climbing robot based on five-bar mechanisms. *Ocean Eng.* **2024**, *298*, 117140. [CrossRef]
25. Liu, T.; Fan, X. The Force Analysis of High Pressure Water Jet Cleaning Machine Theory. *Clean. World* **2008**, *24*, 26–29.
26. Wu, Z.; Liu, L.; Lu, C.; Liu, Y.; Liu, T.; Fan, X. Analysis and Study of Parameters in High Pressure Water Jet Cleaning Steel Plate System. *Metall. Equip.* **2009**, *6*, 60–65.
27. Zhao, Z.; Tao, Y.; Wang, J.; Hu, J. The multi-objective optimization design for the magnetic adsorption unit of wall-climbing robot. *J. Mech. Sci. Technol.* **2022**, *36*, 305–316. [CrossRef]
28. Li, Z.; Fan, J. Design and analysis of a climbing robot for weld detection. *J. Phys. Conf. Ser.* **2022**, *2365*, 012029. [CrossRef]
29. Xiong, D.; Liu, Y.L. Force analysis and stability simulation on tracked wall-climbing robot. *J. Mech. Electr. Eng.* **2015**, *32*, 929–932.
30. Wen, C. *Crawling Characteristics Analysis and Control System Design of Complex Wall Cleaning Robot*; Zhejiang University of Technology: Hangzhou, China, 2019.

Disclaimer/Publisher's Note: The statements, opinions and data contained in all publications are solely those of the individual author(s) and contributor(s) and not of MDPI and/or the editor(s). MDPI and/or the editor(s) disclaim responsibility for any injury to people or property resulting from any ideas, methods, instructions or products referred to in the content.